Dimolybdenum paddlewheel complexes with cation binding sites as electrolyte additives to manipulate the solid-electrolyte interphase at lithium metal anodes

Simon G. Gersib,[a] Erik J. Askins,[a,b] Matthew Li,[b] S. M. Supundrika Subasinghe,[a] Biki Kumar Behera,[a,b] Dan McElheny,[a] Seoung-Bum Son,[b] Khalil Amine,[b] Ksenija D. Glusac,[a,b] Neal P. Mankad*,[a]

[a] Department of Chemistry, University of Illinois Chicago, 845 W. Taylor St., Chicago, IL 60607, USA

[b] Chemical Sciences and Engineering Division, Argonne National Laboratory, 9700 Cass Ave, Lemont, IL 60439, USA

* npm@uic.edu

Abstract

Use of electrolyte additives at mM loadings to control the surface chemistry of lithium metal anodes (LMAs) is a leading strategy to improve safety, efficiency, and reliability of lithium metal batteries and promote various types of electrosynthetic reactions. Whereas previous studies employed either inorganic or organic additives, in this study we report the first organometallic additive, $Mo_2(mea)_4$ [**1**, mea = 2-(2-methoxyethoxy)acetate], a dimolybdenum paddlewheel complex that is stable under Li plating conditions. Unlike more classically used crown ether additives, complex **1** features cation binding sites in the second coordination sphere that promote reversible Li^+ coordination. Furthermore, binding of Li^+ ions to **1** induces aggregation of cationically charged coordination oligomers/polymers that assemble at the LMA surface due to electrostatic attraction. Upon surface immobilization and incorporation into the solid-electrolyte interphase (SEI), the additive serves multiple beneficial functions. It was found to protect the LMA against parasitic side reactions by chemical passivation, produce modest but measurable improvements to Li plating properties (e.g. overpotential, surface structure, Coulombic efficiency), and modulate the composition and thickness of the SEI. The latter effect translates to significantly decreased resistance in battery settings due to improved interfacial charge transport properties. The most notable benefit to battery cycling performance comes from calendar aging tests, which show that the presence of the additive protects the LMA from parasitic side reactions that would otherwise decrease overall cell cycling efficiency Collectively, these data disclose a new tactic for designing electrolyte additives using principles of organometallic synthesis.

Introduction

Whereas ubiquitous lithium-ion batteries use graphitic anodes to host Li^+ ions in the charged state, several next-generation battery schemes will depend on hostless lithium metal anodes (LMAs) that boast high specific capacities (3860 mAh g^{-1}) and low potentials (-3.04 V *vs.* SHE) necessary to enable a vertical leap in the energy density of rechargeable batteries.[1,2] The adoption of devices with LMAs has faced impediments primarily related to safety risks, including the potential for short circuits and thermal runaway, that stem from unwanted Li dendrites growing on the anode surface during Li plating (charging) and stripping (discharging) cycles. Additionally, capacity fade due to parasitic side reactions at the highly reactive LMA surface remains a problem for lithium metal batteries (LMBs).[2–4] Use of LMAs also extends beyond batteries to other applications such as electroreduction of N_2 to NH_3,[5] a commodity chemical critical to sustaining the human population.[6] Therefore, it is critical to identify strategies enabling control of Li plating and stripping processes and protection of the anode from spontaneous reactions with the electrolyte.

Improving the stability of LMBs and/or controlling surface reactivity of LMAs hinges on controlling the solid-electrolyte interphase (SEI). This critical layer that forms natively on the reactive LMA surface stabilizes the electrode-electrolyte interface by preventing direct contact between the reducing Li metal and the reducible electrolyte. The SEI must be mechanically robust, allowing for lithium ion and charge transport processes while accommodating LMA volume changes during battery cycling.[3] Specific electrolytes have been employed to create robust SEIs, with lithium bis(trifluoromethanesulfonyl)imide (LiTFSI) and lithium bis(fluorosulfonyl)imide (LiFSI) emerging as leading candidates.[7,8] The beneficial effects of these electrolyte components are attributed to their decomposition at the LMA surface into LiF-rich SEIs, a phenomenon known to increase the stability of LMBs by impeding dendrite formation and promoting lithium ion transport characteristics.[9] While crystalline LiF has poor Li^+ transport properties, amorphous LiF, especially when doped with lithiophilic impurities, has the potential for fast Li^+ transport.[10,11] Thus, although LiF-rich SEI layers tend to be beneficial, having SEIs that are too rich in LiF negatively impacts battery performance.[12] In other words, optimizing the ratio of LiF to other SEI components is critical. Therefore, identifying ways to precisely control SEI composition is also of great interest. Strategies being investigated to selectively deposit optimal SEI compositions include electrolyte design,[13] electrode manipulation,[13] and use of electrolyte additives.[14] Additives have a rich history of improving battery life and functionality in lithium-ion batteries[15] and many additives have been explored to enhance LMA properties.[14] Of particular relevance to this study, recent works have demonstrated beneficial effects of crown ethers (e.g., 15-crown-5, 18-crown-6) as electrolyte additives.[16–19]

Electrolyte additives are typically classified as either purely inorganic (e.g. $LiNO_3$, $LiAsF_6$, $AlCl_3$) or purely organic (e.g. vinylene carbonate, fluoroethylene carbonate).[20] In this study, we report what we believe to be the first organometallic additive species. The additive is based on the so-called "paddlewheel" motif that typically consists of a binuclear (M···M) metal unit spanned by four bridging ligands (e.g. carboxylates) to create a 4-fold symmetric environment (e.g. $[M_2(OAc)_4]^{n+}$). These bimetallic paddlewheel complexes represent a privileged motif in coordination chemistry and have applications in catalysis,[21–23] medicine,[24] and investigations of fundamental bonding concepts.[25–27] Among these compounds, Group VI complexes such as $Mo_2(OAc)_4$ have played an important role in developing knowledge of metal-metal bonding due to their electronic configurations leading to quadruple ($M{\equiv}M = \sigma + 2\pi + \delta$) metal-metal bonds.[28–30] Importantly, the quadruply-bonded paddlewheel complexes are known to be stable even at potentials relevant to Li plating.[31,32] As part of our investigations of second coordination sphere effects on these dimolybdenum paddlewheels,[33] we decided to install second-sphere cation binding sites into the molecular architecture. Here, we report that one such complex that, when used as an electrolyte additive, not only influences the nature and composition of the SEI but also incorporates itself into the SEI as a lithiophilic species. In doing so, the additive serves several functions including passivation of the LMA toward parasitic side reactions, improvement of Li plating properties, and attenuation of charge transfer resistance. Notably, a significant improvement in battery cycling performance was measured in the presence of the additive during calendar aging tests, indicating that the protection imparted on the LMA toward parasitic side reactions serves a useful and practical benefit.

Results & Discussion

We adapted a literature synthesis of the canonical paddlewheel complex, $Mo_2(OAc)_4$,[34] to prepare the title $Mo_2(mea)_4$ [**1**, mea = 2-(2-methoxyethoxy)acetate] complex on gram scale in >90% yield in a single step from commercially available 2-(2-methoxyethoxy)acetic acid and $Mo(CO)_6$ (Scheme 1). Bulk samples of **1** were characterized by ^1H NMR spectroscopy and elemental analysis (see Supporting Information). Compared to relatively insoluble $Mo_2(OAc)_4$, **1** showed significant solubility in organic solvents like acetonitrile, tetrahydrofuran (THF), dimethyl carbonate, and 1,2-dimethoxyethane (DME, monoglyme). Unlike air-stable $Mo_2(OAc)_4$, **1** underwent air oxidation within seconds of air exposure, converting to an unknown diamagnetic species. Therefore, all subsequent experiments were carried out in inert-atmosphere gloveboxes. The solid-state structure of **1** determined by X-ray crystallography features a

Mo≡Mo bond distance of 2.09891(16) Å, which is quite similar to the corresponding distance of 2.093(1) Å for $Mo_2(OAc)_4$.[35]

Scheme 1. Synthesis of $Mo_2(mea)_4$ (**1**).[a]

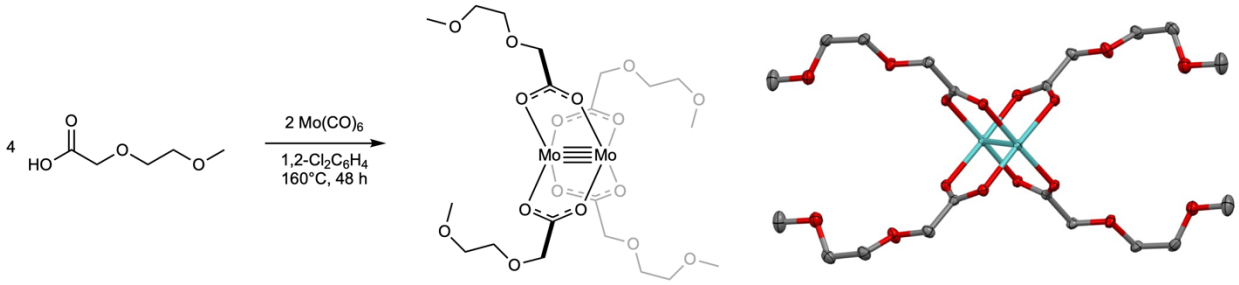

[a] Solid-state structure from X-ray crystallography is shown as 50%-probability thermal ellipsoids (H atoms and a co-crystallized solvent molecule omitted).

Exposure of **1** to various Li^+ salts indicated that the oxygen-rich environment surrounding the dimolybdenum unit in **1** is capable of Li^+ binding, a phenomenon we initially discovered from X-ray crystallography experiments. For example, when attempting to grow crystals of **1** in the presence of $LiBF_4$, we instead obtained crystals of $Mo_2(mea)_4 \cdot 4LiBF_4$ (**2**). The solid-state structure of **2** (Figure 1a) features a 1D chain of $Mo_2(mea)_4$ units in which each mea group has captured a Li^+ ion to give an overall 4:1 Li^+:Mo_2 stoichiometry. In the structure of **2**, each mea ligand has a carboxylate oxygen atom bridging between Mo and Li^+ as well as two ether oxygens chelating Li^+ in a hemi-crown manner. The coordination spheres of each Li^+ are completed by BF_4^- anions, which bridge between Li^+ cations to propagate the 1D chain. The Mo≡Mo bond distance in **2** is 2.0875(9) Å, indicating a shortening of ~0.012 Å from **1** upon Li^+ binding. Such bond contractions can be indicative of changes to the electronic nature of the Mo≡Mo bond via ligand field effects. For example, a Mo≡Mo contraction of similar magnitude was observed when replacing two acetate ligands from $Mo_2(OAc)_4$ with guanidate ligands, which also corresponded to a significant shift in the Mo_2^{5+}/Mo_2^{4+} reduction potential.[36] In this case, the change in Mo≡Mo bond distance likely reflects a change in donor strength of mea upon Li^+ binding.

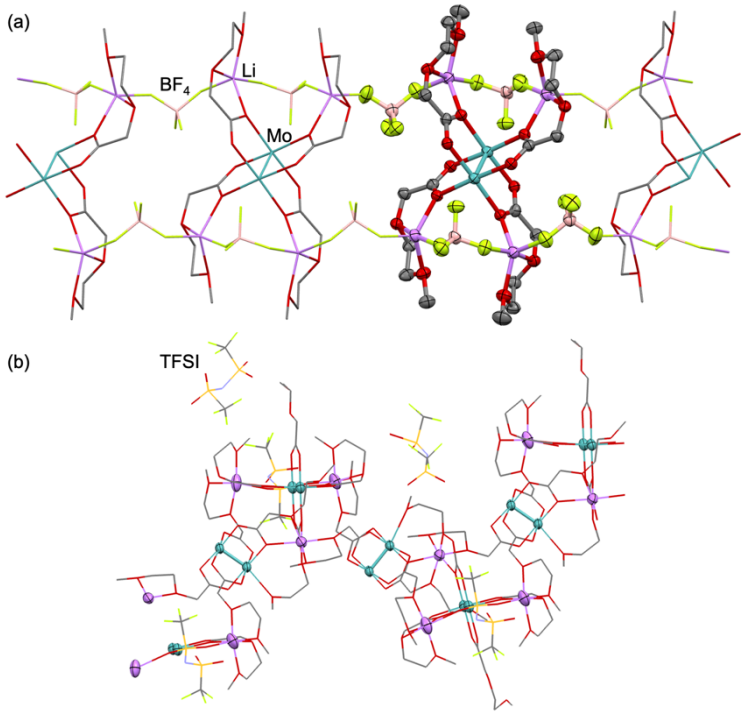

Figure 1. Solid-state structures (polymer expansion views) of (a) $[Mo_2(mea)_4]\cdot 4LiBF_4$ (**2**) and (b) $[Mo_2(mea)_4]\cdot 1.5LiTFSI$ (**3**) determined by X-ray crystallography (selected atoms shown as 50%-probability thermal ellipsoids, H atoms co-crystallized solvent molecules omitted).

Next, similar experiments were conducted with LiTFSI [TFSI = $N(SO_2CF_3)_2^-$], an electrolyte often used in lithium battery cells. Crystals of $Mo_2(mea)_4\cdot n$LiTFSI were grown from solutions in both DME and THF. The solid-state structure from DME (**3**, Figure 1b) features an overall 1.5:1 Li^+:Mo_2 stoichiometry comprising a zig-zag shaped 1D chain. Here, the chain propagates *via* Li^+ cations bound to mea ligands from neighboring $Mo_2(mea)_4$ sub-units. There are also "dangling" Li^+ cations not involved in propagating the chain whose coordination spheres are completed by $TFSI^-$ anions. The coordination polymer backbone is cationically charged, and so there are also outer-sphere $TFSI^-$ anions in the lattice for charge balance. The structure from THF (**4**, Figure S1) is generally like that of **3** and features THF ligands bound to Mo centers along the Mo≡Mo axis.[37] Because these extended coordination polymers depend to some extent on anion moieties bridging between sub-units and/or coordinating "dangling" Li^+ ions in the solid state, it is unlikely that the crystallographic structures reflect solution behavior. Nonetheless, these data imply that, upon Li^+ binding to **1**, coordination oligomers or polymers can form in solution from aggregation via intermolecular mea···Li^+···mea bridging.

^{7}Li NMR measurements were used to establish that Li^+ binding by **1** does occur in solution, as well. Both the chemical shift and the linewidth of the ^{7}Li NMR resonance for LiTFSI were found to change depending on **1**:LiTFSI ratio in solution, with higher **1**:LiTFSI ratios giving more downfield shifted and broadened signals (Figure 2a). Based on literature precedent, the single ^{7}Li NMR resonance observed under all conditions examined can be assigned as the weighted average of bound and unbound Li^+ ions that are in rapid exchange on the NMR timescale.[38] As such, it was not possible to distinguish the four potential Li^+ binding sites in **1** by ^{7}Li NMR spectroscopy in this case.[39] However, the average Li^+ binding constant (K_s) for all the binding sites was determined to be 1.53 ± 0.15 M^{-1} based on this ^{7}Li NMR data (see Supporting Information for derivation). This average binding constant is relatively small compared to non-aqueous cation binding by crown ethers and crown ether-appended transition metal systems even in comparable solvent environments,[40–42] which play a role in Li^+ mobility in the SEI (see below).

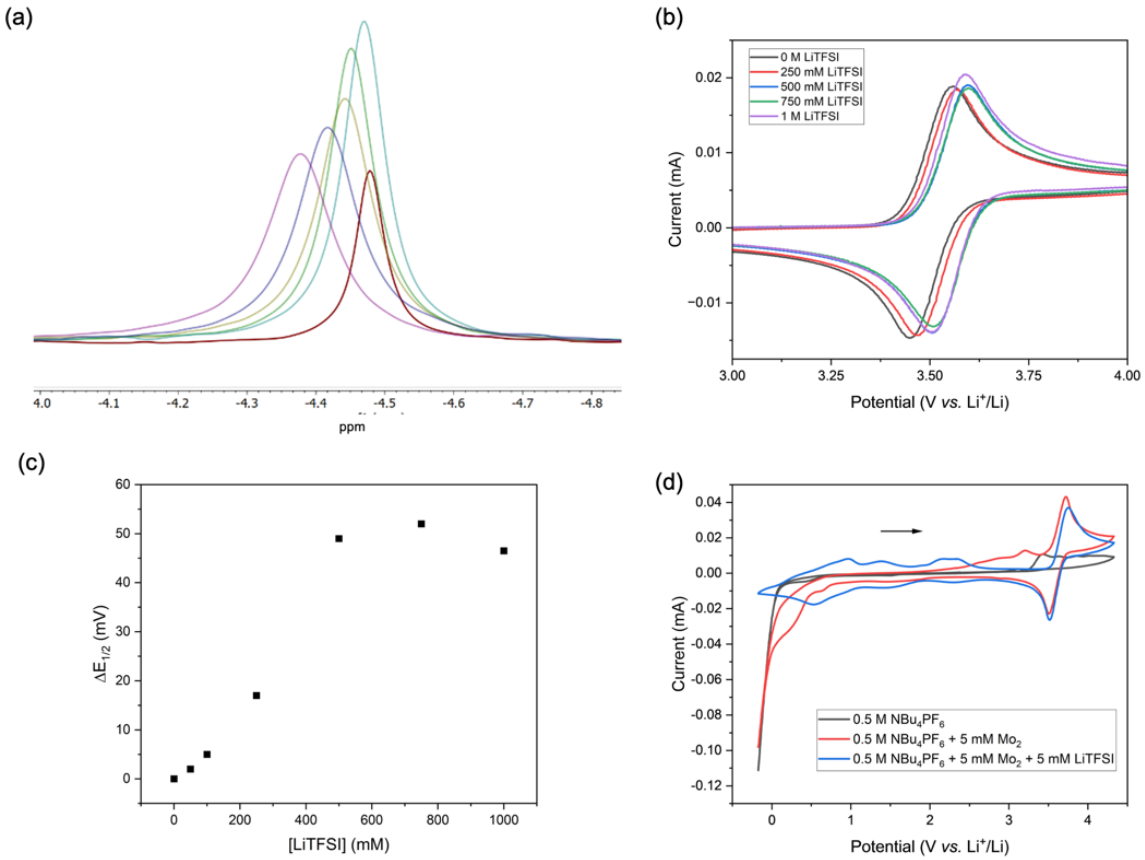

Figure 2. (a) Effect of added $Mo_2(mea)_4$ (**1**) on ^{7}Li NMR spectrum of 5 mM LiTFSI in DME:$CDCl_3$ (4:1) for Mo_2:Li ratios up to 4 (maroon spectrum is of an external LiTFSI standard); (b) effect of LiTFSI on the Mo_2^{5+}/Mo_2^{4+} couple of **1** in mixed LiTFSI/NBu_4OTf electrolytes (1 M total ion concentration in DME); (c) change in half-wave potential for the Mo_2^{5+}/Mo_2^{4+} couple as a function of LiTFSI concentration; (d) demonstration of 5 mM $[Mo_2(mea)_4]\cdot n Li^+$ passivating the working electrode toward bulk $[NBu_4]^+$ reduction (Pt working electrode, 100 mV s^{-1} scan rate).

To probe the individual Li^+ binding sites in **1**, we employed density functional theory (DFT) calculations to analyze the Gibbs free energy changes associated with the simulated reactions represented by equation 1. The first Li^+ binding event (n = 1 in equation 1) was calculated to be roughly thermoneutral (ΔG_1 = 0.1 kcal mol^{-1}), consistent with the weak (reversible) binding indicated by ^{7}Li NMR experiments. Binding a second Li^+ ion (n = 2) is also feasible ($\Delta G_{2\text{-}trans}$ = 4.2 kcal mol^{-1}) provided the two Li^+ ions are bound to mea ligands that are *trans* to one another. However, binding two Li^+ ions in a *cis* orientation or binding a third Li^+ ion (n = 3) were both found to be thermodynamically inaccessible under standard conditions ($\Delta G_{2\text{-}cis}$ = 26.5 kcal mol^{-1} and ΔG_3 = 36.6 kcal mol^{-1}). These calculations indicate that, on average, each molecule of **1** will bind ≤ 2 Li^+ ions in solution while always maintaining a *trans* disposition between Li^+ ions to minimize charge repulsion.

$$Mo_2(mea)_4 + n[Li(DME)_2]^+ \rightarrow [Mo_2(mea)_4\cdot n Li]^{n+} + 2n DME \qquad \text{(eq 1)}$$

Next, we carried out exploratory cyclic voltammetry (CV) measurements, motivated by previous observations that cation binding sites impact the reduction potentials and reactivity profiles of transition metal complexes.[43–45] Dimolybdenum paddlewheels are known to show excellent electrochemical and

chemical redox reversibility by CV associated with the δ-bonding electrons.[28] Accordingly, the CV of **1** (5 mM in 0.5 M LiTFSI/DME) showed a reversible (Figures S11-S13) redox event at 3.53 V vs. Li^+/Li that is assigned to the Mo_2^{5+}/Mo_2^{4+} couple. When CV measurements for **1** were conducted in a mixed LiTFSI/NBu_4OTf electrolyte (1.0 M total ion concentration in DME, Figure 2b), the half-wave potential ($E_{1/2}$) value was found to depend on LiTFSI concentration, with the shift in half-wave potential ($\Delta E_{1/2}$) moving to more positive potentials with increasing [LiTFSI]. At concentrations of [LiTFSI] > 400 mM, the $\Delta E_{1/2}$ plateaued at ~50 mV (Figure 2c). The fact that $\Delta E_{1/2}$ is relatively small in this case is attributed, in part, to the weak binding of Li^+ by **1**. For comparison, $\Delta E_{1/2}$ > 100 mV is typically observed for crown ether-functionalized transition metal systems with significantly stronger cation binding characteristics.[42,43] In this regard, the behavior observed by CV coincides with conclusions reached from ^{7}Li NMR measurements and DFT calculations.

Figure 2d shows the influences of **1** and/or LiTFSI additives on the CV of NBu_4PF_6 (0.5 M in dimethylcarbonate) electrolyte. The CV in the absence of additives showed electrolyte reduction onset at ~0 V vs. Li^+/Li. Upon adding **1** (5 mM) to this electrolyte, new small features of unknown origin were observed at ~0.25 and ~0.5 V in addition to the reversible $[Mo_2]^{5+}/[Mo_2]^{4+}$ couple at 3.5 V, but there was only a minimal effect on the electrolyte reduction profile at ~0 V. However, to our surprise, the presence of both **1** and LiTFSI at low loadings (5 mM each) completely suppressed reduction of the bulk electrolyte near ~0 V. Our interpretation of these results is that the interaction of **1** and LiTFSI produces some $[Mo_2(mea)_4 \cdot nLi]^{n+}$ species (or aggregate thereof) that dramatically influences electrode surface chemistry, in this case effectively expanding the potential window of the electrolyte by passivating the working electrode towards $[NBu_4]^+$ reduction. Characterization of surface species will be discussed below.

Inspired by these observations and the previous literature on crown ethers as electrolyte additives,[16–19] we went on to examine effects of **1** on Li plating/stripping behavior. In initial experiments (e.g. Figure S15), CV scans were swept anodically starting at open-circuit potential (~3 V vs. Li^+/Li), which allowed for the observation of the reversible Mo_2^{5+}/Mo_2^{4+} redox event in the first cycle that effectively served as an internal current and potential standard. Upon passing through Li plating and stripping potentials and re-scanning anodically in subsequent cycles, not only was the Mo_2^{5+}/Mo_2^{4+} couple maintained, but also its current and peak shape changed in a manner that was dependent on the electrolyte (LiTFSI vs. LiFSI; FSI = $N(SO_2F)_2^-$), solvent (mono- vs. tetraglyme), and working electrode (Pt vs. glassy carbon). From these observations, we concluded that (a) solution-phase **1** is robust even under Li plating conditions, and (b) some type of electrocatalytic reaction occurs at the Mo_2^{5+}/Mo_2^{4+} potential, presumably involving solution-phase **1** promoting transformation(s) of electrolyte component(s) or degradation product(s) thereof. Although solution-phase electrocatalysis at these potentials is beyond the scope of lithium metal anode chemistry, a thorough analysis of this data set is presented in Supporting Information.

Data presented in Figure 3 focuses on the CV region associated with Li plating and stripping. In the absence of additives, CV experiments with LiFSI (1 M in DME) showed clear plating and stripping waves that were monitored over 50 cycles (Figure 3a). The maximum stripping current (~0.9 mA) was observed at Cycle 1. By Cycle 10, the stripping current faded to its minimum value of 0.55 mA. Subsequently, stripping current increased then stabilized at ~0.6 mA by Cycle 50. Over 50 CV cycles in the presence of **1** (5 mM), the stripping current started at ~0.8 mA, dropped to ~0.5 mA, then stabilized at ~0.6 mA (Figure 3b). Thus, overall, the effect of additive **1** on stripping current is deleterious at Cycle 1 (Figure 3c) before converging to behavior that is nearly indistinguishable from the baseline case (Figure 3d). More significant changes were evident when examining Li plating overpotentials. The presence of **1** increased plating overpotential by ~20 mV at Cycle 1 (Figure 3c) but then decreased it over time such that, by Cycle 50, the overpotential was smaller with additive **1** than without (Figure 3d). On the other hand, stripping overpotentials were seemingly unaffected in these experiments. The slope of the stripping wave's rising edge was slightly less steep in the presence of **1**, indicating that the additive slows Li stripping rates.[46,47] Overall, the presence of additive **1** does not block Li plating/stripping despite its

chemical passivation of the working electrode, and it also has a modest but measurable beneficial effect on Li plating overpotential once a stable SEI has been established over the first few cycles.[46]

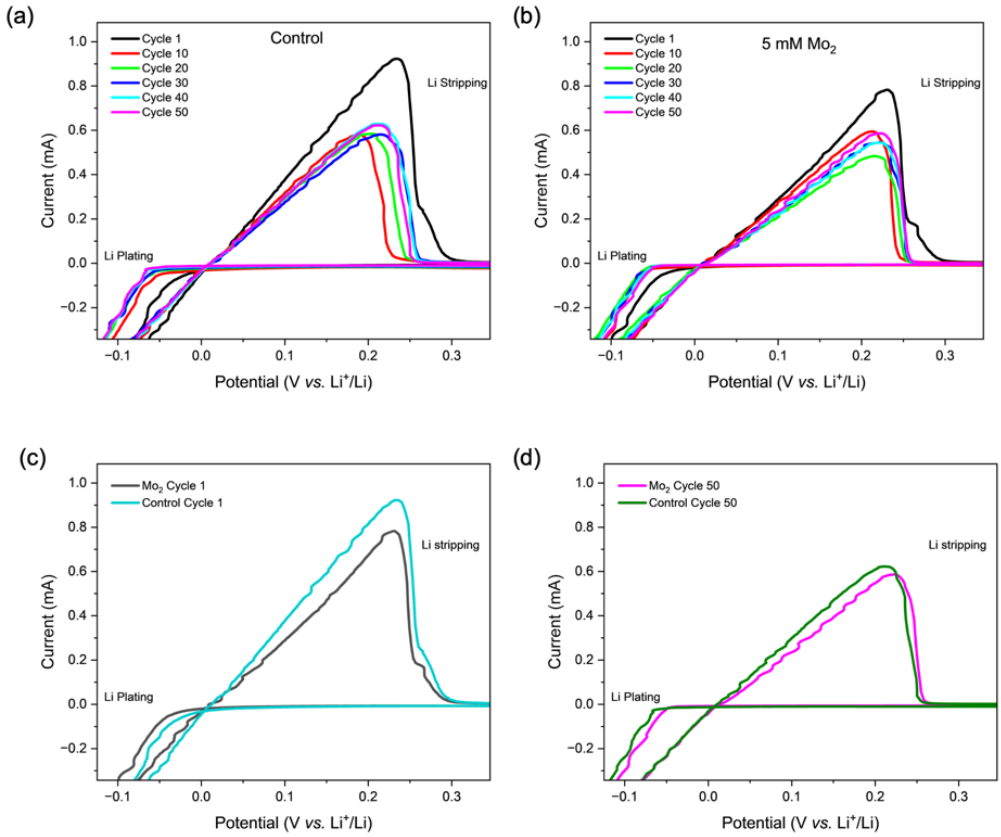

Figure 3. Comparisons of Li plating and stripping behavior of LiFSI (1 M in DME) examined by CV (Pt working electrode, 10 mV s^{-1}) with and without additive **1** (5 mM).

Next, a Cu||Li coin cell reservoir method established by Adams *et. al.*[48] was used to examine the effect of **1** as an additive in a more realistic lithium metal battery setting. According to this method, after a Cu surface conditioning plating/stripping step, a Li reservoir was plated on a Cu working electrode, then a fraction of Li was stripped and plated in each cycle, and finally the entire reservoir was stripped in the last cycle. The final amount of stripped Li divided by the initial reservoir amount plated was used as a representative Coulombic efficiency (CE) value, on average, for the ensemble of cycles conducted. Several coin cell conditions were screened (Figure S27), and LiFSI at 4 M concentration in DME with **1** as an additive at ≤3 mM concentrations were identified as suitable conditions for further experimentation. Using these conditions, an extended protocol with smaller (i.e., faster) plating and stripping cycles was employed to efficiently examine longer term effects (Figure 4a).[48] Here, while the average CE remained constant regardless of additive concentration (Figure 4b), the overpotentials for Li nucleation and growth varied depending on [**1**]. The electrolyte mixture with no additive showed larger overpotentials both initially and throughout the experiment compared to the case with 1 mM **1** as an additive (Figure 4c). While the nucleation overpotential returned to its baseline value when additive concentration increased to 3 mM, the overpotential for growth maintained a lower value even at the higher additive loading. Overall, these coin cell experiments are aligned with the CV experiments discussed above in that they indicate

modest but measurable changes to overpotentials induced by additive **1**, which presumably promotes deposition of a surface layer with slightly lower resistance than the native SEI.

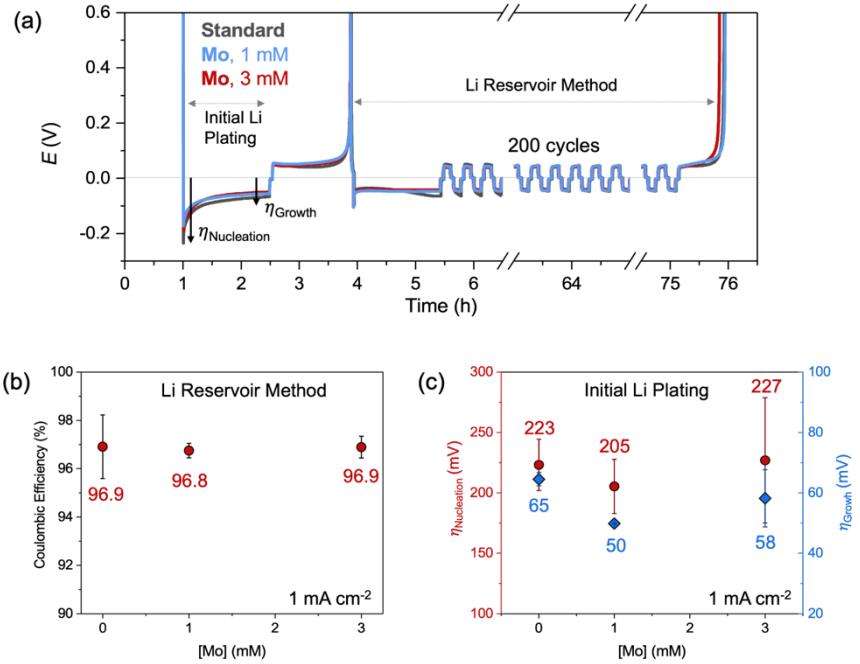

Figure 4. Effect of additive **1** on Cu||Li half-cell cycling: (a) charge/discharge profile following a protocol with initial long Li plating/stripping cycles on Cu followed by 200 rapid cycles then complete stripping of the Li reservoir; (b) average Coulombic efficiency as a function of additive concentration; (c) nucleation and growth overpotentials as functions of additive concentration.

Several of the behaviors observed during CV and coin cell measurements imply that $[Mo_2(mea)_4 \cdot n\text{Li}]^{n+}$ (or a derivative thereof) impacts the nature of the SEI and/or incorporates into the SEI structure. Therefore, the Li anodes from the Cu||Li coin cells described above were washed with DME after completion of the cycling experiments and analyzed by X-ray photoelectron spectroscopy (XPS). Whereas Li content was constant regardless of whether **1** was used as an additive (Figure 5a), major differences in F and Mo content were evident by XPS. In the absence of additive **1**, features were observed at 685 and 689 eV that are assigned to the F 1*s* binding energies of LiF and organofluorine (–CF) species, respectively.[7,9,12,49] In the presence of 1 mM **1**, only the 685-eV feature for LiF was observed and the organofluorine peak was absent (Figure 5b). These results imply that low loadings of **1** as an electrolyte additive influence SEI formation substantially, here suppressing organofluorine deposition and favoring LiF formation. (The specific effects on SEI composition are highly electrolyte dependent; see, for example, Figure S28.) A larger ratio of LiF to –CF can be indicative of a thinner SEI, as inorganics such as LiF tend to be found at higher concentrations near the anode surface.[12,50] For the cell with 1 mM **1**, the presence of immobilized Mo was also evident by XPS (Figure 5c). Two features at 232 and 235 eV were observed that are assigned to the Mo $3d_{5/2}$ and $3d_{3/2}$ binding energies, respectively, of the surface-bound species. Metallic Mo or surface Mo alloys are expected to have Mo $3d_{5/2}$ binding energies of ~228 eV,[49] whereas $Mo_2(OAc)_4$ was previously reported to have a binding energy of 232 eV.[51] The presence of Mo centers in a higher oxidation state than Mo(0) metal suggests that the surface Mo species in these experiments have intact Mo≡Mo bonds rather than having undergone reduction to the metallic Mo^0 state, even at the extreme potentials of a Li metal anode. Taken together, it can be concluded that use of **1** as an

electrolyte additive both dramatically influences the nature and composition of the SEI and results in incorporation of discrete Mo≡Mo species into the SEI structure.

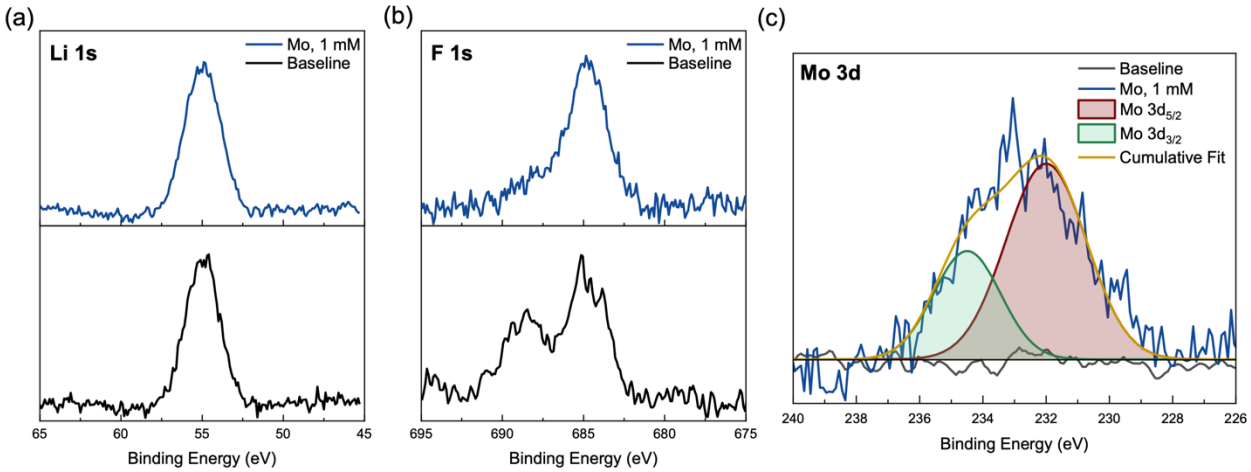

Figure 5. XPS characterization of the anode surface after extended cycling focusing on the (a) Li 1*s*, (b) F 1*s*, and (c) Mo 3*d* binding energies. Baseline curves indicate cells with no additive.

The anode surfaces from the Cu||Li coin cells were further analyzed by scanning electron microscopy (SEM). In both the control conditions and an experiment with 3 mM **1** in 4 M LiFSI/DME, Li plating was observed to have started at the edges and grown toward the center of the anode (Figure S30), which is likely due to a non-uniform distribution previously reported for coin cells.[52] When the anodes were examined after one conditioning cycle and one lithium plating step, it was evident that the plated Li exhibited a smoother surface with fewer small, feather-like features in the presence of additive **1** (Figure 6a) compared to the control (Figure 6b). However, after extended cycling (200 cycles), the two SEM images showed quite similar morphologies (Figure S33).

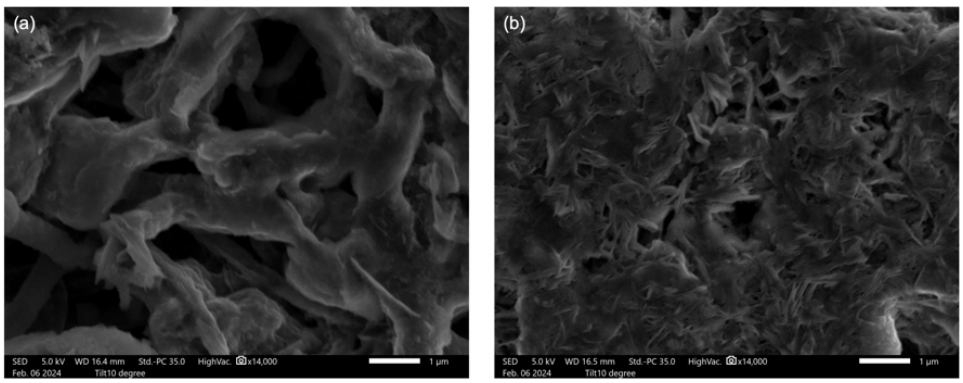

Figure 6. SEM characterization (14000x magnification) of anode surfaces after 1 charge step (4 M LiFSI/DME) of a Cu||Li cell showing surface morphology of plated Li with (a) 3 mM **1** additive, and (b) no additive.

To further probe the nature of the SEI, we conducted cycling experiments in symmetric Li||Li cells and periodically performed electrochemical impedance spectroscopy (EIS) measurements. Charge/discharge

profiles with and without 3 mM **1** additive were monitored over 300 cycles each (Figure 7a). In the first few cycles, measurable changes in cycling profile and overpotentials were noted in the presence of **1** (Figure 7b). Figure 7c shows the net additive effect of **1** on Li plating overpotential ($\eta_{Mo} - \eta_{baseline}$). At the first plating cycle, the overpotential of the Mo-containing cell produced an overpotential that was markedly worse than that of the baseline (~100 mV larger). However, at the 10th cycle, the overpotential of the baseline cell began to exceed that of the 3 mM **1** cell and maintained a slightly higher overpotential up to 300 cycles. This effect of 3 mM **1** aligns nicely with the CV experiments which suggested beneficial effects on Li plating/stripping overpotentials resulting from the presence of additive **1**.

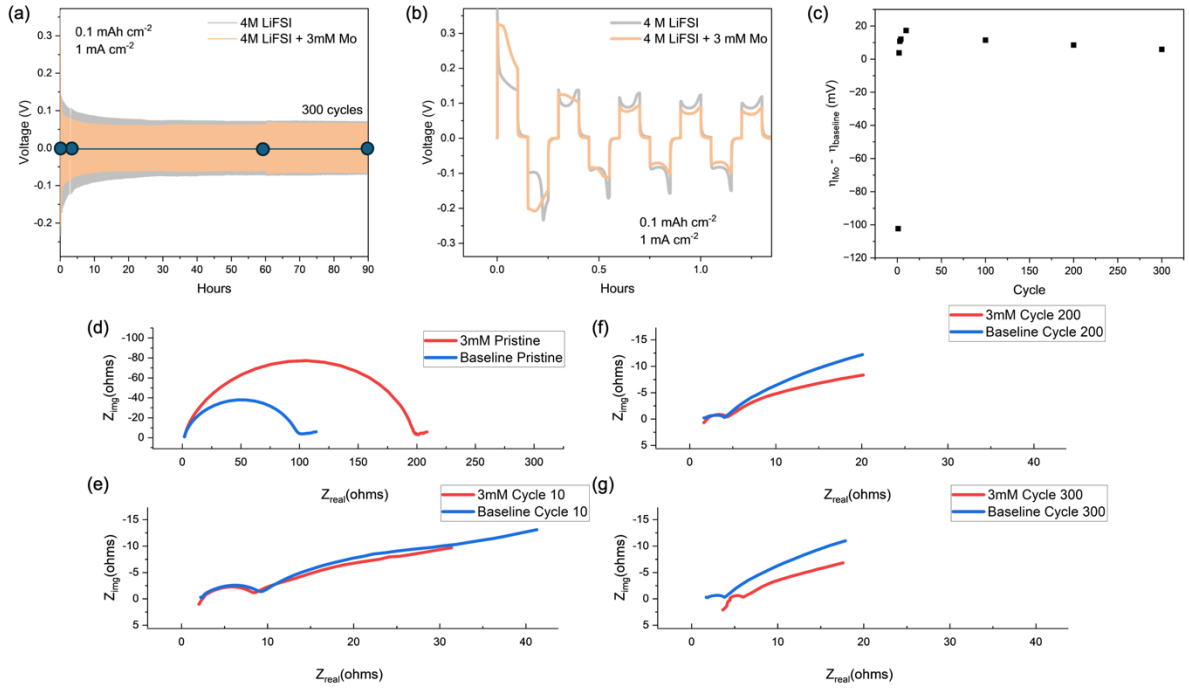

Figure 7. Effect of additive **1** (3 mM) on Li||Li coin cell cycling: (a) charge/discharge profile over 300 cycles with blue circles indicating time points at which EIS measurements were taken; (b) charge/discharge profile for the first 4 cycles highlighting effect of additive **1** on overpotential; (c) net additive effect on plating overpotential as a function of cycle number; EIS measurements (d) before cycling, (e) at Cycle 10, (f) at Cycle 200, and (g) at Cycle 300.

In an effort to understand the working mechanism of 3 mM **1** during cycling, EIS measurements were also conducted at the points indicated by circles in Figure 7a.[53] When examining pristine cells before cycling, there was significantly more impedance with additive **1** compared to the baseline case (Figure 7d). This indicates that, upon exposure of **1** to the cell at OCP even before cycling, there is already *in-situ* formation of $[Mo_2(mea)_4 \cdot nLi]^{n+}$ complexes and/or oligomers that localize at the anode surface and act as insulating SEI components. We attribute both the spontaneous assembly on the anode surface and the insulating behavior to the positive charge of the additive/Li^+ complex and the resulting electrostatic shielding effect.[16,17,50,54] In support of this working model, we conducted a separate experiment in which a Li||Li coin cell was left at OCP for 7 h, during which EIS measurements were taken every 30 min (Figures S34-S38). In the absence of additive **1**, as expected,[53] impedance grew over time as the Li reacts with the electrolyte. Surprisingly, in the presence of additive **1** (3 mM), impedance decreased over time. The decrease does not vary linearly with $t^{0.5}$ as is commonly observed for growing SEI layers during storage (Figure S36 vs. Figure S37).[55] Interestingly, the decrease in impedance fits to an exponential decay,

perhaps indicating this phenomenon is governed by a first order process (Figure S38). We suspect that the source of this decrease in impedance is related to some activation process of **1** (as seen in the symmetric cell cycling), which requires a reaction/adsorption step. This process is likely to be first order kinetically. However, more detailed analysis is required to elucidate the mechanism.

Nevertheless, EIS data taken at different cycles revealed that the addition of **1** has a positive impact in terms of decreasing overall impedance. Cycles 10 (Figure 7e), 200 (Figure 7f), and 300 (Figure 7g) with and without additive were nearly superimposable in the high-frequency region, indicating that additive **1** appears not to impact ion transport properties of the SEI.[53] Substantial differences were evident at the mid- and low-frequency regions, which nominally should report on charge transfer and diffusion in bulk electrolyte, respectively. However, after cycling, Li electrodes are often transformed from planar surfaces to high surface-area porous morphologies.[26] Hence, the Li-ion diffusion impedance also probes the diffusion through this porous SEI/non-planar Li matrix. The interpretation of the broad low frequency half-semicircle likely includes a closed Warburg transmissive boundary[58] with non-reflective electrodes such as Li. Additive **1** apparently lowers resistance toward charge transfer and/or mass transport. Direct attempts to deconvolute the charge transfer resistance from diffusion resistance through the SEI/Li-matrix (*via* equivalent circuit modeling) was not successful due to the overlap in frequency. However, their trends with cycling could be more revealing of their relative importance. As Li metal is never considered to be plated in a planar manner,[59] the Li-ion diffusion impedance is expected to only increase with cycling (i.e., the Li electrode becomes thicker and more tortuous with cycling). However, Figure 7e (10^{th} cycle) clearly indicates a low frequency impedance that is larger than that of Figures 7f-g (200^{th} and 300^{th} cycles), suggesting that the diffusion impedance contribution from the SEI/Li matrix is not dominating. The fact that the impedance decreases with cycling indicates that the plating of fresh, high surface-area Li metal is occurring (since impedance is inversely proportion to electrochemically active surface area), and its impact on impedance likely overshadows any impact of the diffusion impedance from the SEI/Li matrix. Thus, additive **1** plays an important role in enhancing charge transfer. As the observed differences in impedance could stem from differing electrochemically active surface structures rather than from incorporation of **1** decreasing charge transfer resistance, it was important to confirm that the surface areas are roughly the same between the two samples. The relative surface area increase were gauged by comparing the relative decrease in impedance for the high-frequency semi-circle (SEI impedance), which clearly shows a similar impedance drop from the 10^{th} cycle (Figure 7e) to 200^{th} and 300^{th} cycles (Figures 7f-g) for both electrolyte mixtures. This indicates that surface area increase is roughly the same between the two electrolyte. Because the surface areas were roughly similar according to this analysis, the impedance of the cell containing additive **1** being lower than baseline is attributed to the ability of **1** to decrease charge transfer resistance.

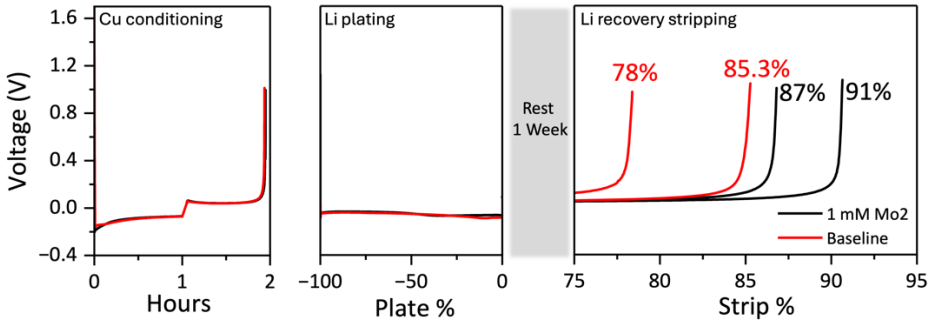

Figure 8. Voltage profiles for Cu||Li coin cells subjected to 1-week aging tests at 1 mA cm^{-2}.

If **1** forms a molecular layer over the Li surface, it might also provide better protection of the anode than a heterogeneous passivation layer with non-zero porosity (i.e., SEI) toward spontaneous reactions with electrolyte. Some indication of such behavior was already discussed above (e.g., Figure 2d). Accordingly, we briefly explored the impact of **1** on calendar aging of Li metal anodes (Figure 8). In these experiments, a reservoir of Li was plated onto Cu electrodes, left for a certain amount of time to allow for the cell to "calendar age", then stripped off. Like the CE experiments above, the CE was calculated by dividing the final lithium stripped by the reservoir of plated lithium (Figure 8, middle panel). The CE after 1 week (Figure 8) was 87-91% with additive **1** (3 mM) and 78-85% in the control condition of 4 M LiFSI in DME. These preliminary aging results suggest that **1** chemically and/or electrostatically shields the electrode, similar to the effect observed with crown ethers and other additives[14,17] and in good agreement with cycling and EIS data discussed above.

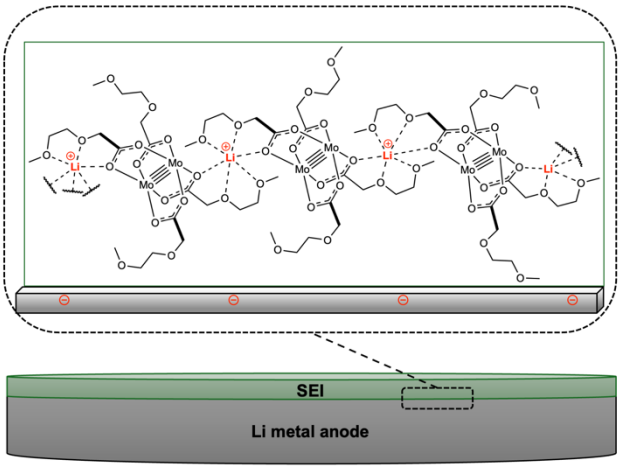

Figure 9. Schematic of the $Mo_2(mea)_4$-modified SEI in this study.

Conclusions

The title complex, $Mo_2(mea)_4$ (**1**), was studied as an electrolyte additive in the context of lithium metal batteries. In solution, ^{7}Li NMR spectroscopy and cyclic voltammetry indicated that the Li^+ binding sites in the second coordination sphere of **1** have small binding constants and rapidly exchange Li^+ ions with the bulk solution. According to X-ray crystallography, Li^+ binding to **1** can also induce aggregation to generate cationically charged coordination oligomers/polymers. Several observations including XPS characterization imply that these cationic aggregates spontaneously assemble electrostatically on lithium metal anode surfaces (Figure 9), wherein they dramatically impact the nature and composition of the solid-electrolyte interphase (SEI). Specifically, additive **1** promotes selective decomposition of LiFSI into a LiF-rich SEI that also contains the additive, itself, without reduction to metallic Mo^0. The modified SEI was shown to be chemically passivated towards parasitic reactions with electrolyte according to cyclic voltammetry and calendar aging experiments, show modest improvements to Li plating properties (i.e., overpotential, surface structure) according to electrochemical cycling and surface microscopy measurements, and exhibit decreased impedance due to improved interfacial charge transport properties according to electrochemical impedance spectroscopy. The benefit appears to increase with cycling (to some extent), indicating some activation/formation process in the functioning mechanism of the $Mo_2(mea)_4$. Although the individual effects of the additive are modest in some cases, the ensemble of these effects leads to significant improvement in battery cycling performance after calendar aging. Furthermore, this report represents the first use of an organometallic species as an electrolyte additive,

thus opening a new design space for development in this frontier area expected to impact next-generation energy storage devices.

Acknowledgments

Funding was provided by the National Science Foundation under grants CHE-2350403 and CHE-1954298 to N.P.M. and K.G., respectively. Computational resources and services were provided by the Advanced Cyberinfrastructure for Education and Research (ACER) group at UIC. Prof. Jordi Cabana (UIC) provided useful suggestions and access to an argon glovebox. The authors gratefully acknowledge support of this work from the U.S. Department of Energy (DOE), Office of Energy Efficiency and Renewable Energy, Vehicle Technologies Office. Argonne National Laboratory is operated for the U.S. DOE, Office of Science, by UChicago Argonne, LLC, under Contract No. DE-AC02-06CH11357.

References

(1) Liu, J.; Bao, Z.; Cui, Y.; Dufek, E. J.; Goodenough, J. B.; Khalifah, P.; Li, Q.; Liaw, B. Y.; Liu, P.; Manthiram, A.; Meng, Y. S.; Subramanian, V. R.; Toney, M. F.; Viswanathan, V. V.; Whittingham, M. S.; Xiao, J.; Xu, W.; Yang, J.; Yang, X.-Q.; Zhang, J.-G. Pathways for Practical High-Energy Long-Cycling Lithium Metal Batteries. *Nat. Energy* **2019**, *4* (3), 180–186. https://doi.org/10.1038/s41560-019-0338-x.

(2) Cheng, X.-B.; Zhang, R.; Zhao, C.-Z.; Zhang, Q. Toward Safe Lithium Metal Anode in Rechargeable Batteries: A Review. *Chem. Rev.* **2017**, *117* (15), 10403–10473. https://doi.org/10.1021/acs.chemrev.7b00115.

(3) Liu, D.-H.; Bai, Z.; Li, M.; Yu, A.; Luo, D.; Liu, W.; Yang, L.; Lu, J.; Amine, K.; Chen, Z. Developing High Safety Li-Metal Anodes for Future High-Energy Li-Metal Batteries: Strategies and Perspectives. *Chem. Soc. Rev.* **2020**, *49* (15), 5407–5445. https://doi.org/10.1039/C9CS00636B.

(4) Xu, W.; Wang, J.; Ding, F.; Chen, X.; Nasybulin, E.; Zhang, Y.; Zhang, J.-G. Lithium Metal Anodes for Rechargeable Batteries. *Energy Env. Sci* **2014**, *7* (2), 513–537. https://doi.org/10.1039/C3EE40795K.

(5) Chang, W.; Jain, A.; Rezaie, F.; Manthiram, K. Lithium-Mediated Nitrogen Reduction to Ammonia via the Catalytic Solid–Electrolyte Interphase. *Nat. Catal.* **2024**, *7* (3), 231–241. https://doi.org/10.1038/s41929-024-01115-6.

(6) Lehnert, N.; Musselman, B. W.; Seefeldt, L. C. Grand Challenges in the Nitrogen Cycle. *Chem. Soc. Rev.* **2021**, *50* (6), 3640–3646. https://doi.org/10.1039/d0cs00923g.

(7) Wang, M.; Huai, L.; Hu, G.; Yang, S.; Ren, F.; Wang, S.; Zhang, Z.; Chen, Z.; Peng, Z.; Shen, C.; Wang, D. Effect of LiFSI Concentrations To Form Thickness- and Modulus-Controlled SEI Layers on Lithium Metal Anodes. *J. Phys. Chem. C* **2018**, *122* (18), 9825–9834. https://doi.org/10.1021/acs.jpcc.8b02314.

(8) Zhang, H.; Shen, C.; Huang, Y.; Liu, Z. Spontaneously Formation of SEI Layers on Lithium Metal from LiFSI/DME and LiTFSI/DME Electrolytes. *Appl. Surf. Sci.* **2021**, *537*, 147983. https://doi.org/10.1016/j.apsusc.2020.147983.

(9) Fan, X.; Ji, X.; Han, F.; Yue, J.; Chen, J.; Chen, L.; Deng, T.; Jiang, J.; Wang, C. Fluorinated Solid Electrolyte Interphase Enables Highly Reversible Solid-State Li Metal Battery. *Sci. Adv.* **2018**, *4* (12), eaau9245. https://doi.org/10.1126/sciadv.aau9245.

(10) Basu, S.; Hwang, G. S. Amorphization of Inorganic Solid Electrolyte Interphase Components and Its Impact on Enhancing Their Transport and Mechanical Properties. *ACS Appl. Mater. Interfaces* **2023**, *15* (51), 59494–59501. https://doi.org/10.1021/acsami.3c14279.

(11) Li, Y.; Li, Y.; Zhang, L.; Tao, H.; Li, Q.; Zhang, J.; Yang, X. Lithiophilicity: The Key to Efficient Lithium Metal Anodes for Lithium Batteries. *J. Energy Chem.* **2023**, *77*, 123–136. https://doi.org/10.1016/j.jechem.2022.10.026.

(12) Zhou, S.; Zhu, Y.; Hu, H.; Li, C.; Jiang, J.; Huang, J.; Zhang, B. Tuning the LiF Content in the SEI by Engineering the Molecular Structures of Porous Organic Polymers for Solid-State Lithium Metal Batteries. *J. Mater. Chem. A* **2023**, *11* (11), 5636–5644. https://doi.org/10.1039/D2TA09896B.
(13) Zhang, S.; Yang, G.; Liu, S.; Li, X.; Wang, X.; Wang, Z.; Chen, L. Understanding the Dropping of Lithium Plating Potential in Carbonate Electrolyte. *Nano Energy* **2020**, *70*, 104486. https://doi.org/10.1016/j.nanoen.2020.104486.
(14) Zhang, H.; Eshetu, G. G.; Judez, X.; Li, C.; Rodriguez-Martínez, L. M.; Armand, M. Electrolyte Additives for Lithium Metal Anodes and Rechargeable Lithium Metal Batteries: Progress and Perspectives. *Angew. Chem. Int. Ed.* **2018**, *57* (46), 15002–15027. https://doi.org/10.1002/anie.201712702.
(15) Zhang, S. S. A Review on Electrolyte Additives for Lithium-Ion Batteries. *J. Power Sources* **2006**, *162* (2), 1379–1394. https://doi.org/10.1016/j.jpowsour.2006.07.074.
(16) Xu, W.; Xiao, J.; Wang, D.; Zhang, J.; Zhang, J.-G. Crown Ethers in Nonaqueous Electrolytes for Lithium/Air Batteries. *Electrochem. Solid-State Lett.* **2010**, *13* (4), A48. https://doi.org/10/d83dc9.
(17) Zhao, J.; Li, Q.; Pang, Y.; Lu, Z.; Wu, J.; Zhao, X.; Lou, X.; Yang, S.; Liu, Y.; Qiao, Y. Introducing Crown Ether as a Functional Additive for High-Performance Dendrite-Free Li Metal Batteries. *ACS Appl. Energy Mater.* **2021**, *4* (8), 7829–7838. https://doi.org/10.1021/acsaem.1c01174.
(18) Wang, H.; He, J.; Liu, J.; Qi, S.; Wu, M.; Wen, J.; Chen, Y.; Feng, Y.; Ma, J. Electrolytes Enriched by Crown Ethers for Lithium Metal Batteries. *Adv. Funct. Mater.* **2021**, *31* (2), 2002578. https://doi.org/10/gg4tpp.
(19) Zhang, Q.; Rao, S.; Vummaleti, S. V. C.; Poh, E. T.; Dai, W.; Cui, X.; Wu, J.; Zhang, J.; Chen, W. High-Performance Li-O $_2$ Batteries Enabled by Dibenzo-24-Crown-8 Aldehyde Derivative as Electrolyte Additives. *Adv. Energy Mater.* **2022**, *12* (26), 2200580. https://doi.org/10/gs2hhz.
(20) Wu, B.; Chen, C.; Raijmakers, L. H. J.; Liu, J.; Danilov, D. L.; Eichel, R.-A.; Notten, P. H. L. Li-Growth and SEI Engineering for Anode-Free Li-Metal Rechargeable Batteries: A Review of Current Advances. *Energy Storage Mater.* **2023**, *57*, 508–539. https://doi.org/10.1016/j.ensm.2023.02.036.
(21) Powers, D. C.; Ritter, T. Bimetallic Redox Synergy in Oxidative Palladium Catalysis. *Acc. Chem. Res.* **2012**, *45* (6), 840–850. https://doi.org/10.1021/ar2001974.
(22) Hansen, J.; Davies, H. M. L. High Symmetry Dirhodium(II) Paddlewheel Complexes as Chiral Catalysts. *Coord. Chem. Rev.* **2008**, *252* (5–7), 545–555. https://doi.org/10/d73v2w.
(23) Berry, J. F. Metal–Metal Multiple Bonded Intermediates in Catalysis. *J. Chem. Sci.* **2015**, *127* (2), 209–214. https://doi.org/10.1007/s12039-015-0773-6.
(24) Tolbatov, I.; Barresi, E.; Taliani, S.; La Mendola, D.; Marzo, T.; Marrone, A. Diruthenium(II , III) Paddlewheel Complexes: Effects of Bridging and Axial Ligands on Anticancer Properties. *Inorg. Chem. Front.* **2023**, *10* (8), 2226–2238. https://doi.org/10/gt6zg3.
(25) Harisomayajula, N. V. S.; Makovetskyi, S.; Tsai, Y.-C. Cuprophilic Interactions in and between Molecular Entities. *Chem. – Eur. J.* **2019**, *25* (38), 8936–8954. https://doi.org/10/gssz57.
(26) Berry, J. F. Two-Center/Three-Electron Sigma Half-Bonds in Main Group and Transition Metal Chemistry. *Acc. Chem. Res.* **2016**, *49* (1), 27–34. https://doi.org/10/gt6zg5.
(27) Rej, S.; Tsurugi, H.; Mashima, K. Multiply-Bonded Dinuclear Complexes of Early-Transition Metals as Minimum Entities of Metal Cluster Catalysts. *Coord. Chem. Rev.* **2018**, *355*, 223–239. https://doi.org/10.1016/j.ccr.2017.08.016.
(28) Cotton, F. A.; Murillo, C. A.; Walton, R. A. *Multiple Bonds between Metal Atoms*, 3rd ed.; Springer: New York, 2005.
(29) Cotton, F. A. Centenary Lecture: Quadruple Bonds and Other Multiple Metal to Metal Bonds. *Chem. Soc. Rev.* **1975**, *4* (1), 27–53. https://doi.org/10.1039/CS9750400027.
(30) Falvello, L. R.; Foxman, B. M.; Murillo, C. A. Fitting the Pieces of the Puzzle: The δ Bond. *Inorg. Chem.* **2014**, *53* (18), 9441–9456. https://doi.org/10.1021/ic500119h.
(31) Cotton, F. A.; Gruhn, N. E.; Gu, J.; Huang, P.; Lichtenberger, D. L.; Murillo, C. A.; Van Dorn, L. O.; Wilkinson, C. C. Closed-Shell Molecules That Ionize More Readily than Cesium. *Science* **2002**, *298* (5600), 1971–1974. https://doi.org/10.1126/science.1078721.

(32) Chiarella, G. M.; Cotton, F. A.; Durivage, J. C.; Lichtenberger, D. L.; Murillo, C. A. Solubilizing the Most Easily Ionized Molecules and Generating Powerful Reducing Agents. *J. Am. Chem. Soc.* **2013**, *135* (47), 17889–17896. https://doi.org/10.1021/ja408291k.
(33) Subasinghe, S.; Mankad, N. Quantifying Effects of Second-Sphere Cationic Groups on Redox Properties of Dimolybdenum Quadruple Bonds. *Chem. Commun.* **2024**. https://doi.org/10.1039/D4CC02759K.
(34) Brignole, A. B.; Cotton, F. A.; Dori, Z.; Dori, Z.; Dori, Z.; Wilkinson, G. Rhenium and Molybdenum Compounds Containing Quadruple Bonds. In *Inorganic Syntheses*; John Wiley & Sons, Ltd, 1972; pp 81–89. https://doi.org/10.1002/9780470132449.ch15.
(35) Robbins, G. A.; Martin, D. S. Crystal Structures of Tetrakis (.Mu.-Formato)Dimolybdenum(II)-Potassium Chloride and Two New Polymorphs of Tetrakis(.Mu.-Formato)Dimolybdenum(II). Single-Crystal Optical Absorption Spectra for Systems with the Molybdenum(II) Formate Dimers. *Inorg. Chem.* **1984**, *23* (14), 2086–2093. https://doi.org/10.1021/ic00182a021.
(36) Rodríguez-López, N.; Metta, N.; Metta-Magana, A. J.; Villagrán, D. Redox Potential Tuning of Dimolybdenum Systems through Systematic Substitution by Guanidinate Ligands. *Inorg. Chem.* **2020**, *59* (5), 3091–3101. https://doi.org/10.1021/acs.inorgchem.9b03394.
(37) Dolinar, B. S.; Berry, J. F. Lewis Acid Enhanced Axial Ligation of [Mo2]4+ Complexes. *Inorg. Chem.* **2013**, *52* (8), 4658–4667. https://doi.org/10.1021/ic400275x.
(38) Peters, S. J.; Stevenson, C. D. The Complexation of the Na+ by 18-Crown-6 Studied via Nuclear Magnetic Resonance. *J. Chem. Educ.* **2004**, *81* (5), 715–717. https://doi.org/10.1021/ed081p715.
(39) Thordarson, P. Determining Association Constants from Titration Experiments in Supramolecular Chemistry. *Chem Soc Rev* **2011**, *40* (3), 1305–1323. https://doi.org/10.1039/C0CS00062K.
(40) Danil De Namor, A. F.; Ng, J. C. Y.; Llosa Tanco, M. A.; Salomon, M. Thermodynamics of Lithium−Crown Ether (12-Crown-4 and 1-Benzyl-1-Aza-12-Crown-4) Interactions in Acetonitrile and Propylene Carbonate. The Anion Effect on the Coordination Process. *J. Phys. Chem.* **1996**, *100* (34), 14485–14491. https://doi.org/10.1021/jp960519a.
(41) Schmidt, E.; Popov, A. I.; Kintzinger, J. P.; Tremillon, J.-M. Nuclear Magnetic Resonance and Calorimetric Studies on the Solvation of Cryptand C221 and Its Sodium(+) and Potassium(+) Ion Complexes in Nonaqueous Solvents. *J. Am. Chem. Soc.* **1983**, *105* (26), 7563–7566. https://doi.org/10.1021/ja00364a016.
(42) Miller, A. J. M. Controlling Ligand Binding for Tunable and Switchable Catalysis: Cation-Modulated Hemilability in Pincer-Crown Ether Ligands. *Dalton Trans.* **2017**, *46* (36), 11987–12000. https://doi.org/10.1039/C7DT02156A.
(43) Kang, K.; Fuller, J.; Reath, A. H.; Ziller, J. W.; Alexandrova, A. N.; Yang, J. Y. Installation of Internal Electric Fields by Non-Redox Active Cations in Transition Metal Complexes. *Chem. Sci.* **2019**, *10* (43), 10135–10142. https://doi.org/10.1039/C9SC02870F.
(44) Reath, A. H.; Ziller, J. W.; Tsay, C.; Ryan, A. J.; Yang, J. Y. Redox Potential and Electronic Structure Effects of Proximal Nonredox Active Cations in Cobalt Schiff Base Complexes. *Inorg. Chem.* **2017**, *56* (6), 3713–3718. https://doi.org/10/f9th65.
(45) Chantarojsiri, T.; Reath, A. H.; Yang, J. Y. Cationic Charges Leading to an Inverse Free-Energy Relationship for N−N Bond Formation by MnVI Nitrides. *Angew. Chem. Int. Ed.* **2018**, *57* (43), 14037–14042. https://doi.org/10/gfcx9k.
(46) Vanhoutte, G.; Brooks, N. R.; Schaltin, S.; Opperdoes, B.; Van Meervelt, L.; Locquet, J.-P.; Vereecken, P. M.; Fransaer, J.; Binnemans, K. Electrodeposition of Lithium from Lithium-Containing Solvate Ionic Liquids. *J. Phys. Chem. C* **2014**, *118* (35), 20152–20162. https://doi.org/10.1021/jp505479x.
(47) Qian, J.; Henderson, W. A.; Xu, W.; Bhattacharya, P.; Engelhard, M.; Borodin, O.; Zhang, J.-G. High Rate and Stable Cycling of Lithium Metal Anode. *Nat. Commun.* **2015**, *6* (1), 6362. https://doi.org/10.1038/ncomms7362.

(48) Adams, B. D.; Zheng, J.; Ren, X.; Xu, W.; Zhang, J. Accurate Determination of Coulombic Efficiency for Lithium Metal Anodes and Lithium Metal Batteries. *Adv. Energy Mater.* **2018**, *8* (7), 1702097. https://doi.org/10.1002/aenm.201702097.
(49) Justin Gorham. NIST X-Ray Photoelectron Spectroscopy Database - SRD 20, 2012. https://doi.org/10.18434/T4T88K.
(50) Shan, X.; Zhong, Y.; Zhang, L.; Zhang, Y.; Xia, X.; Wang, X.; Tu, J. A Brief Review on Solid Electrolyte Interphase Composition Characterization Technology for Lithium Metal Batteries: Challenges and Perspectives. *J. Phys. Chem. C* **2021**, *125* (35), 19060–19080. https://doi.org/10.1021/acs.jpcc.1c06277.
(51) Best, S. A.; Squires, R. G.; Walton, R. A. The X-Ray Photoelectron Spectra of Heterogeneous Catalysts: III. Catalysts Derived from Dimeric Molybdenum(II) Carboxylates on Silica and Their Reactions with Carbon Monoxide, Nitric Oxide, and Hydrogen. *J. Catal.* **1979**, *60* (2), 171–183. https://doi.org/10.1016/0021-9517(79)90140-4.
(52) Shea, J.; Huang, X.; Li, M.; Son, S.-B.; Su, C.-C.; Liu, T.; Dong, P.; Chen, A.; Yang, L.; Luo, C.; Amine, K.; Janakiraman, U. Impact of Pressure Distribution and Magnitude on the Performance of Lithium Metal Anodes. *J. Electrochem. Soc.* **2024**, *171* (2), 020528. https://doi.org/10/gt6v5s.
(53) Srout, M.; Carboni, M.; Gonzalez, J.; Trabesinger, S. Insights into the Importance of Native Passivation Layer and Interface Reactivity of Metallic Lithium by Electrochemical Impedance Spectroscopy. *Small* **2023**, *19* (7), 2206252. https://doi.org/10.1002/smll.202206252.
(54) Ding, F.; Xu, W.; Graff, G. L.; Zhang, J.; Sushko, M. L.; Chen, X.; Shao, Y.; Engelhard, M. H.; Nie, Z.; Xiao, J.; Liu, X.; Sushko, P. V.; Liu, J.; Zhang, J.-G. Dendrite-Free Lithium Deposition via Self-Healing Electrostatic Shield Mechanism. *J. Am. Chem. Soc.* **2013**, *135* (11), 4450–4456. https://doi.org/10.1021/ja312241y.
(55) Attia, P. M.; Chueh, W. C.; Harris, S. J. Revisiting the $t^{0.5}$ Dependence of SEI Growth. *J. Electrochem. Soc.* **2020**, *167* (9), 090535. https://doi.org/10/gt6v5t.
(56) Jow, T. R.; Delp, S. A.; Allen, J. L.; Jones, J.-P.; Smart, M. C. Factors Limiting Li+ Charge Transfer Kinetics in Li-Ion Batteries. *J. Electrochem. Soc.* **2018**, *165* (2), A361. https://doi.org/10.1149/2.1221802jes.
(57) Bieker, G.; Winter, M.; Bieker, P. Electrochemical in Situ Investigations of SEI and Dendrite Formation on the Lithium Metal Anode. *Phys. Chem. Chem. Phys.* **2015**, *17* (14), 8670–8679. https://doi.org/10/gfrgb5.
(58) Lazanas, A. Ch.; Prodromidis, M. I. Electrochemical Impedance Spectroscopy─A Tutorial. *ACS Meas. Sci. Au* **2023**, *3* (3), 162–193. https://doi.org/10/gtkp5f.
(59) Owensby, K. D.; Sahore, R.; Tsai, W.-Y.; Chen, X. C. Understanding and Controlling Lithium Morphology in Solid Polymer and Gel Polymer Systems: Mechanisms, Strategies, and Gaps. *Mater. Adv.* **2023**, *4* (23), 5867–5881. https://doi.org/10/gt6v5w.